A METHODOLOGY TO PREDICT THE GAS PERMEABILITY PARAMETERS OF TIGHT RESERVOIRS FROM NITROGEN SORPTION ISOTHERMS AND MERCURY POROSIMETRY CURVES

Christos D. Tsakiroglou[1], Adnan Al Hinai[2], Reza Rezaee[2]
[1]Foundation for Research and Technology Hellas – Institute of Chemical Engineering Sciences, Stadiou str., Platani, 26504 Patras, Greece
[2]Department of Petroleum Engineering, Curtin University, Perth, WA, Australia

This paper was prepared for presentation at the International Symposium of the Society of Core Analysts held in Trondheim, Norway, 27-30 August 2018

ABSTRACT
For the explicit computation of the absolute permeability and Knudsen diffusion coefficient of tight rocks (shales) from pore structure properties, a methodology is suggested. The pore space is represented by a pore-and-throat network quantified by bimodal pore and throat size distributions, pore shape factors, and pore accessibility function. With the aid of percolation theory analytic equations are developed to express the N_2 adsorption / desorption isotherms and Hg intrusion curve as functions of all pertinent pore structure parameters. A multistep procedure is adopted for the successive estimation of each set of parameters by the inverse modeling of N_2 adsorption, N_2 desorption, and Hg intrusion datasets. With the aid of critical path analysis of percolation theory, approximate relationships are developed allowing the explicit calculation of the absolute permeability and Knudsen diffusion coefficient, from estimated pore network properties. Application of the methodology to the datasets of several shale samples enables us to evaluate the predictability of the approach.

INTRODUCTION
Tight and shale reservoir systems pose a tremendous potential resource for future development, and study of these systems is proceeding apace. In particular, shale gas reservoirs possess many so-called "unconventional" features and considerations on macro- and micro-scales of flow, and their extremely low permeability presents unusual challenges [4, 6]. Particularly, the tools of traditional production data analysis have not been sufficient for determining the reservoir matrix permeability in these unconventional systems. Depending on the pore size range, the flow of natural gas through porous conventional rocks, tight formations and shale systems, is dominated by a variety of flow regimes, including Knudsen, transition, slip and viscous Darcy flow [13]. Knowledge and understanding of rock properties, including pore geometry, permeability, and fluid distribution are essential for determining shale's hydrocarbon storage and recovery. The microstructural characterization of shale samples could be achieved by combining

mercury injection capillary pressure (MICP), with low-field nuclear magnetic resonance (NMR), nitrogen adsorption/desorption (N_2) and high resolution focused ion beam–scanning electron microscopy (FIB–SEM) images [1]. The gas permeability of shales can be correlated with the capillary pressure data from mercury injection measurements, by using theoretical and empirical equations [2]. On the other hand, the pore network approach is a practical way to explain the macro flow behavior of porous media from a microscopic point of view, and the shale matrix can be simulated by 3-dimensional pore network models that include typical bimodal pore size distribution, anisotropy and low connectivity [12]. Moreover, the digital rock with nanopores could be constructed by 3D pore structure images obtained from micro/nano CT and FIB-SEM images reconstructed from 2D SEM images of pore structure, and using the Lattice Boltzmann method to calculate the intrinsic permeability, porosity and tortuosity; these parameters are used to calculate the apparent permeability under consideration of different combined gas transport mechanisms [9]. In the present work, with the aid of percolation theory, analytic models of the N_2 adsorption-desorption isotherms and Hg intrusion curves as functions of the pore and throat radius distributions and pore network connectivity are developed [10]. Then a stepwise methodology is adopted to estimate the pore network parameters with inverse modeling of N_2 sorption and Hg intrusion curves and applied to datasets of several shale samples. The critical path analysis of percolation theory is used to calculate the liquid permeability and Knudsen diffusion coefficient of porous media explicitly from the aforementioned pore structure parameters and compare the predictions with experimental measurements.

METHODS AND MATERIALS

Pore-scale models of drainage and imbibition

The pore structure is represented by a stochastic network of pores (sites)-and-throats (bonds), the sizes of which are sampled from bimodal site $f_s(r)$ and bond radius $f_b(r)$ distribution functions. The throats are considered as narrow constrictions without volume, while the pores are assigned the entire pore volume according to the relation

$$V_s(r) \propto r^{\beta_s} \tag{1}$$

where β_s is a volume shape factor ($\beta_s \geq 0$). The cross-section of each pore is modeled by a high-order regular polygon with number of sides (angles), area, and perimeter equal to n_s, A, and P, respectively. The pore shape factor, G, is given by [10]

$$G = A/P^2 \tag{2}$$

and the pore radius, r, is defined as the radius of the inscribed circle in the regular polygon, given by

$$r = 2GP \tag{3}$$

From the polygon geometry, we obtain

$$G = 1/\left[4n_s \tan\left(\pi/n_s\right)\right] \tag{4}$$

The radii of pores follow a bimodal distribution function composed of log-normal component distribution functions, $f_s(r;\langle r_{s1}\rangle,\sigma_{s1},\langle r_{s2}\rangle,\sigma_{s2},c_s)$, where $\langle r_{si}\rangle$, σ_{si}, c_s are the

mean radius, standard deviation, and contribution fraction of component distribution *i* to the overall one. Respectively, the radii of throats ("windows") connecting adjacent pores follow an analogous bimodal distribution function $f_b(r;<r_{b1}>,\sigma_{b1},<r_{b2}>,\sigma_{b2},c_b)$.

Models of N_2 adsorption / desorption in pore-and-throat networks

In general, the filling of pores with liquid nitrogen is carried out through two parallel mechanisms: (1) multilayer surface adsorption of gas molecules on the flat pore-walls and (2) capillary condensation of liquid on the rough regions of the adsorbed layer. The thickness of the adsorbed layer, t_c, is determined by the generalized FHH equation [3]

$$t_c = \sigma\left[b/ln\left(1/x\right)\right]^{1/s} \tag{5}$$

where x is the relative vapor pressure, σ is the diameter of N_2 molecule (σ=3.54 A), b is a parameter depending on the properties of the adsorbent and adsorptive, and s is an index with values ranging from 2 to 3. The curvature radius of the liquid/vapor menisci of the condensate, r_c, is given by Kelvin equation [3]

$$r_c = c/ln\left(1/x\right) \qquad c = V_L^0\gamma_{LG}/RT \tag{6}$$

For the sake of clarity and physical inspection of the produced equations, the fluid saturation is first calculated for $\beta_s = 2.0$ and then the equations are generalized to any β_s value. The saturation of a partially liquid N_2-occupied pore consists of the adsorbed and condensed phases and is given by

$$S_{f2}\left(r,r_c\right) = \left\{4F_{LG}Gr_c^{\,2} + 2r\sigma\left(b/c\right)^{1/s} r_c^{\,1/s} - \left[\sigma\left(b/c\right)^{1/s} r_c^{\,1/s}\right]^2\right\}\Big/r^2 \tag{7}$$

where F_{LG} is the fraction of the pore cross-section area occupied by the wetting fluid (liquid N_2) and depending on its contact angle, θ_{LG} (for liquid N_2, $\theta_{LG}=0^o$, unless otherwise stated). Assuming that any changes of fluid volume in a pore are described by a relation analogous to Eq.(1), Eq.(7) can be read as

$$S_{f2}\left(r,r_c\right) = \left\{4F_{LG}Gr_c^{\,\beta_s} + 2r\sigma\left(b/c\right)^{1/s} r_c^{\,1/s} - \left[\sigma\left(b/c\right)^{1/s} r_c^{\,1/s}\right]^{\beta_s}\right\}\Big/r^{\beta_s} \tag{\8}$$

The capillary condensation in a pore is analogous to wetting fluid (liquid N2) imbibition, and the critical curvature radius of condensation, $r_c = r_{con}$, is given by

$$r_{con} = \left(r - t_c\right)\Big/\left\{4G\left[F_{LG} + \left(\pi - n_s\theta\right)\right]\right\} \text{ if } \quad F_{LG} \geq 0 \quad \text{and} \quad \theta \leq \pi/n_s \tag{9a}$$

$$r_{con} = \left(r - t_c\right)/2\cos\theta_{LG} \quad \text{if} \quad F_{LG} < 0 \quad \text{and} \quad \theta > \pi/n_s \tag{9b}$$

Eq.(9), in conjunction with Eqs.(5) and (6), yield the critical radius $r = r_s$, given by

$$r_s = 4G\left[F_{LG} + \left(\pi - n_s\theta\right)\right]r_{con} + \sigma\left(b/c\right)^{1/s} r_{con}^{\,1/s} \quad \text{if} \quad F_{LG} \geq 0 \quad \text{and} \quad \theta \leq \pi/n_s \tag{10a}$$

$$r_s = 2\cos\theta_{LG}r_{con} + \sigma\left(b/c\right)^{1/s} r_{con}^{\,1/s} \quad \text{if} \quad F_{LG} < 0 \quad \text{and} \quad \theta > \pi/n_s \tag{10b}$$

The liquid nitrogen saturation of a pore network as a function of the relative vapor pressure can be expressed by the relation

$$S_{LN2}(x)=\left[\int_0^{r_s} f_s(r)V_s(r)dr+\int_{r_s}^{\infty} f_s(r)V_s(r)S_{f2}(r)dr\right]\Bigg/\int_0^{\infty} f_s(r)V_s(r)dr \quad (11)$$

The capillary evaporation from a pore is analogous to the wetting fluid (liquid N_2) drainage, and hence the critical curvature radius of evaporation, r_{evp}, is given by

$$r_{evp}=(r-t_c)\frac{\cos\theta_{LG}-\sqrt{\cos^2\theta_{LG}-4F_{LG}G}}{4F_{LG}G} \quad \text{if} \quad F_{LG}\geq 0 \text{ and } \theta\leq\pi/n_s \quad (12a)$$

$$r_{evp}=\frac{(r-t_c)}{2\cos\theta_{LG}} \quad \text{if} \quad F_{LG}<0 \text{ and } \theta>\pi/n_s \quad (12b)$$

which in conjunction with Eqs.(5) and (6) result in

$$r_b=\frac{4F_{LG}Gr_{evp}}{\left(\cos\theta_{LG}-\sqrt{\cos^2\theta_{LG}-4F_{LG}G}\right)}+\sigma(b/c)^{1/s}r_{evp}{}^{1/s} \quad \text{if } F_{LG}\geq 0 \text{ and } \theta\leq\pi/n_s \quad (13a)$$

$$r_b=2\cos\theta_{LG}r_{evp}+\sigma(b/c)^{1/s}r_{evp}{}^{1/s} \quad \text{if } F_{LG}<0 \text{ and } \theta>\pi/n_s \quad (13b)$$

where r_b is the critical radius for N_2 evaporating from throats with $r\geq r_b$. N_2 desorbs from a pore if its radius is less than the critical size (r_b or r_s) and has access either to the bulk vapor phase (primary desorption) or to isolated vapor pockets (secondary desorption). At any stage of the desorption process, the fraction of bonds (throats) q_b and sites (pores) q_s which are "allowable" to the vapor phase are given by

$$q_b=\int_{r_b}^{\infty} f_b(r)dr \quad \text{and} \quad q_s=\int_{r_s}^{\infty} f_s(r)dr \quad (14)$$

respectively. The fraction of accessible sites (pores), Y_{si}, to the vapor phase as a function of the fraction of allowable bonds (throats), q_b, is the pore accessibility function of the network, and according to percolation theory [10, 11], it is affected by the network topology, spatial pore size correlations and network size. $Y_{si}(q_b)$ is a sigmoid curve, the inflection point of which, defines the percolation threshold q_{bc}. Finally, the liquid N_2 saturation during desorption is given by [10]

$$S_{LN2}(x)=\frac{\int_0^{r_s} f_s(r)V_s(r)dr+\frac{q_s-Y_{si}(q_b)}{q_s-q_{si}}\int_{r_s}^{r_{si}} f_s(r)V_s(r)dr+\frac{Y_{si}(q_b)}{q_s}\int_{r_s}^{\infty} f_s(r)V_s(r)S_{f2}(r)dr}{\int_0^{\infty} f_s(r)V_s(r)dr} \quad (15)$$

Model of Hg Intrusion in pore-and-throat network

In general, the value of pore volume calculated from N_2 sorption does not coincide to the corresponding value calculated from Hg intrusion curve. Although Hg is a non-wetting fluid for the majority of materials, by 'convention' the Hg contact angle, θ_{Hg}, is measured with respect to the wetting fluid (low pressure air) and is considered always lower than

90^o. In order to estimate a unique pore volume value, V_p (cm^3/g), the following method is adopted. At a given Hg intrusion contact angle the maximum intrusion capillary pressure is converted to an equivalent relative vapor pressure. This value is interpolated in N_2 desorption curve to calculate the corresponding liquid nitrogen volume. The sum of the two volumes yields the total pore volume. The procedure is repeated for various values of θ_{Hg}, and the produced datasets (V_p vs θ_{Hg}) are fitted to a non-linear parametric function of the form

$$V_p = A_1 + \left(A_2 - A_1\right) \Big/ \left\{1 + 10^{\left[\left(\theta_0 - \theta_{Hg}\right)w\right]}\right\} \tag{16}$$

to estimate the values of A_1,A_2,θ_0, w.

The Hg intrusion in a pore-and-throat network is analogous to capillary evaporation for q_{st}=0 (primary desorption) and is controlled by throat sizes. The mercury saturation in a pore network is given by [10, 11]

$$S_{Hg}\left(P_c\right) = 1 - \frac{\int_0^{r_s} f_s(r)V_s(r)dr + \frac{q_s - Y_{s0}\left(q_b\right)}{q_s}\int_{r_s}^{\infty} f_s(r)V_s(r)dr + \frac{Y_{s0}\left(q_b\right)}{q_s}\int_{r_s}^{\infty} f_s(r)V_s(r)S_{f1}(r)dr}{\int_0^{\infty} f_s(r)V_s(r)dr} \tag{17}$$

where

$$r_c = \gamma_{\mathrm{Hg}} / P_c \qquad F_{Hg} = F\left(\theta \overset{0}{=} \theta_{Hg}\right) \tag{18}$$

$$r_b = \left(4F_{Hg}Gr_c\right) \Big/ \left(\cos\theta_{Hg} - \sqrt{\cos^2\theta_{Hg} - 4F_{Hg}G}\right) \qquad \text{if } F_{Hg} > 0 \text{ or } \theta_{Hg} < \pi/n_s \tag{19a}$$

$$r_b = 2r_c\cos\theta_{Hg} \qquad \text{if} \qquad F_{Hg} < 0 \text{ or } \theta_{Hg} \geq \pi/n_s \tag{19b}$$

Critical path analysis (CPA)

The fluid flow conduction through a pore system with a broad pore size distribution is governed by a critical pore conductance, g_c, which is defined by the condition that all pores with conductance greater than g_c create a network spanning cluster transferring most of the flow [7]. This critical conductance g_c depends on structural characteristics (e.g. pore shape, pore size distribution, connectivity, dimensionality, etc) of the pore space and CPA is used to calculate the corresponding critical pore dimensions. According to CPA [7], all conductances with values greater than g_c are set equal to g_c, while all conductances smaller than g_c are set equal to zero. The transport properties of the critical path may be dominated by universal scaling laws prevailing in the vicinity of the percolation threshold and describing the variation of accessibility function with the fraction of allowed throats [11]. In mathematical terms, the viscous flow or Knudsen flow problem reduces to the calculation of the critical pore dimensions that maximize the total conductance of the critical path [5, 11]. In general, the dependence of the local viscous flow conductance on pore size may be different from that of the local Knudsen diffusion conductance, so that the critical pore dimension may depend on the transport mechanism [11]. The gas molar flux through a porous medium in the transition region between

Knudsen diffusion and viscous flow can be described by the sum of the individual contributions, namely

$$N = -\left(\frac{k_L}{\mu_g}P + D_{kn}\right)\frac{1}{RT}\nabla P \tag{20}$$

where k_L is the liquid permeability, and D_{kn} is the Knudsen diffusion coefficient of the critical path. According to the CPA [11], these properties are approximated by the relationships

$$k_L = \frac{\varphi r^4}{8\langle r_{sq}\rangle^2}\left[q_b(r) - q_{bc}\right]^t \tag{21}$$

$$D_{kn} = c_{kn}\frac{\varphi r^4}{\langle r_{sq}\rangle^2}\left[q_b(r) - q_{bc}\right]^t \qquad c_{kn} = \frac{8}{3}\left(\frac{RT}{2\pi M}\right)^{1/2} \tag{22}$$

where φ is the porosity, t is the universal scaling exponent of conductivity (t=2.0 for 3-D systems), and mean pore radius, $<r_{sq}>$ can be expressed as function of throat radius, r, by

$$\langle r_{sq}\rangle = \int_r^\infty f_s(r)\,dr \tag{23}$$

The values of k_L and D_{kn} are maximized for r = $r_{max,f}$ and r = $r_{max,d}$, respectively. These maximum values are considered approximately equal to the permeability and Knudsen diffusion coefficient of the investigated porous medium.

For low permeable porous media, the measured gas permeability is pressure-dependent and is commonly expressed by the relationship

$$k_g = k_L\left(1 + b/P_m\right) \tag{24}$$

where b is the Klingenberg factor, and P_m is the mean gas pressure [2]. For the steady-state gas flow through a porous medium, the integrated from of Darcy equation, including the Klingenberg effect, takes the form

$$\left(u_2 P_2 L\mu_g\right)/\left(P_m \Delta P\right) = k_L\left(1 + b/P_m\right) \tag{25}$$

where u_2, P_2 are the flow velocity and pressure at the outlet, L is the sample length, μ_g is the gas viscosity, and ΔP is the pressure drop across the sample. By combining Eq.(20) with Eq.(25), it is obtained

$$D_{kn} = \left(bk_L\right)/\mu_g \tag{26}$$

Experimental datasets and multi-step parameter estimation

For the shale samples, the N_2 adsorption/desorption isotherms were measured with Micromeritics TriStar II 3020, whereas the Hg intrusion curve was measured with Micrometrics Autopore IV Porosimeter [1, 2]. The gas permeability and all pertinent Klingenberg parameters were measured with a modified steady-state method, where the sample is embedded in a resin disc and the gas flow rate is measured at the outlet [2]. For the non-linear parameter estimation, numerical codes in the environment of Athena Visual Studio [8] were developed, and a step-wise procedure was adopted. First, the parameters n_s, β_s, and $f_s(r;<r_{s1}>,\sigma_{s1},<r_{s2}>,\sigma_{s2},c_s)$ were estimated with inverse modeling of N_2 adsorption isotherm. Then, the foregoing parameters were fixed, and

$f_b(r;<r_{b1}>,\sigma_{b1},<r_{b2}>,\sigma_{b2},c_b)$ along with $Y_{si}(q_b)$ were estimated with inverse modeling of N_2 desorption isotherm. Then, $Y_{s0}(q_b)$ was estimated from inverse modeling of the Hg intrusion curve. Finally, the throat size distribution, secondary and primary pore accessibility functions, and Hg contact angle were re-estimated, with the simultaneous inverse modeling of N_2 adsorption/desorption isotherms and Hg intrusion curve.

RESULTS AND DISCUSSION

The methodology of the pore structure characterization from N_2 adsorption/desorption isotherms and Hg intrusion curves was applied to datasets of several shale samples (Al Hinai et al., 2013) collected from one well, at various depths, of the Perth Basin (Australia), and the results are shown in Table 1. For one sample (AC5), we were unable to match precisely the Hg intrusion curve (Table 1, Fig.1c/S1), so that the last step of parameter estimation [$f_b(r)$, $Y_{si}(q_b)$, $Y_{s0}(q_b)$, θ_{Hg}] was repeated by changing the initial guesses (Table 1, Fig.1c/S2). Not having imposed any limitation on the pore to the throat size ratio, the estimated throat radius distribution may extend to higher values, compared to the pore radius distribution (Table 1, AC5, S1/S2). The physical interpretation of such a quantitative description is that the throat sizes are comparable to the sizes of interconnecting pores, and probably a simpler model (e.g. a capillary tube network described by only one pore size distribution and one accessibility function) might be more adequate than the present approach for the representation of the pore space. The parameter values estimated from the datasets of all samples were used to compute k_L and D_{kn} (Fig.2) and compare them with corresponding ones from experimental measurements (Table 2). It seems that D_{kn} is predicted satisfactorily for almost all cases (Table 2), while the permeability is almost predictable only for sample AC5, while it fails for AC1 and AC8 (Table 2).

The Knudsen number is commonly used to classify flow regimes in fine pores where deviation from continuum flow is important [13]. It is defined as the ratio of molecular mean free path, λ (nm) to the mean pore radius, r_s (nm), and is given by

$$K_n = \lambda / \langle r_s \rangle \tag{27}$$

If $K_n < 0.01$, then viscous flow dominates, and the conventional fluid dynamics equations and Darcy equation are applicable. If $0.01 < K_n < 0.1$, then slip flow regime occurs and Darcy equation with Klinkenberg or Knudsen modification is applicable. If $0.1 < K_n < 10$, then the transition flow regime prevails, where both slip (continuum) and diffusion flows can occur, and the traditional fluid dynamics equations start to fail. The higher the Knudsen number, the higher the chance of failure. Even though conventional equations could be applied (i.e., Darcy with Knudsen correction), the validity of such a formulation is questionable. It is safer to use Knudsen diffusion equations, especially for flow at higher Knudsen numbers (close to 10). If $K_n > 10$, then the Knudsen (free molecular) flow regime prevails, where the continuum fluid flow equations fully break down, and diffusion-based formulations must be applied. Evidently, for the analyzed samples (Table 2), in the calculation of K_n, the transition (AC5) and Knudsen flow regimes (AC1, AC8) prevail. Therefore, the Knudsen flow is dominant over all cases (AC1, AC5, AC8), but only in the one case (AC5), viscous flow may be evident. Based on the aforementioned

interpretation, failing to predict the value of k_L for AC1 and AC8, and succeeding to predict satisfactorily D_{kn} for all cases seem reasonable.

CONCLUSIONS

Analytical models of Hg intrusion and N_2 adsorption-desorption in porous materials are used for the inverse modeling of experimental datasets of shale samples to estimate a full set of parameters for the pore space, regarded as a pore-and-throat network. Using the critical path analysis of percolation theory, analytical relationships are developed for the explicit computation of the Klinkenberg parameters of the gas permeability from pore space parameters. Application of the methodology to datasets of shales indicates that, based on the estimated pore space parameters, the liquid permeability is predictable at low K_n values, over which the viscous flow regime is valid, while the Knudsen diffusion coefficient is predictable at low and high K_n values, over which Knudsen flow is feasible.

REFERENCES

1. Al Hinai, A.A., Rezaee, R. Pore geometry in gas shale reservoirs. In: *Fundamentals of Gas Shale Reservoirs*, R. Rezaee (ed), pp.89-116 (2015) John Wiley & Sons, Inc.
2. Al Hinai, A.A., Rezaee, R., Saeedi, A., Lenormand, R. Permeability prediction from mercury injection capillary pressure: an example from the Perth Basin, Western Australia. *APPEA J.* (2013) **53**: 31-36.
3. Gregg, S.J., Sing, K.S.W. *Adsorption, Surface Area and Porosity*, Academic Press, London (1982).
4. Hill, D.G., Nelson, C.R. Gas productive fractured shales: an overview and update. *Gas TIP*S (2000) **6**(3): 4–13.
5. Hunt, A.G. Applications of percolation theory to porous media with distributed local conductances. *Adv.Water Resour.* (2001) **24**: 279-307.
6. Javadpour, F., Fisher, D., Unsworth, M. Nanoscale gas flow in shale gas sediments. *J. Can. Pet. Technol.* (2007) **46**(10): 55–61.
7. Katz, A.J., Thompson, A.H., 1986. Quantitative prediction of permeability in porous rock. *Phys. Rev. B* (1986) **34**: 8179-8181.
8. Stewart, W.E., Caracotsios, M. *Computer-Aided Modeling of Reactive Systems*. John Wiley & Sons, Hoboken, New Jersey (2008).
9. Sun, H., Yao, J., Cao, Y-C, Fan, D-Y, Zhang, L. Characterization of gas transport behaviors in shale gas and tight gas reservoirs by digital rock analysis. *Int. J. Heat Mass Transfer* (2017) **104:** 227–239.
10. Tsakiroglou, C.D., Burganos, V.N., Jacobsen, J. Pore structure analysis by using nitrogen sorption and mercury intrusion data. *AIChE J.* (2004) **50**: 489-510.
11. Tsakiroglou, C.D., Ioannidis, M.A., Amirtharaj, E., Vizika, O. A new approach for the characterization of the pore structure of dual porosity rocks. *Chem. Eng. Sci.*, (2004) **64**: 847-859.
12. Zhang, P., Hu, L., Meegoda, J.N. Pore-Scale Simulation and Sensitivity Analysis of Apparent Gas Permeability in Shale Matrix. *Materials* (2017) **10**: 104: 1-13.
13. Ziarani, A.S., Aguilera, R., Knudsen's Permeability Correction for Tight Porous Media. *Transp. Porous Media* (2012) **91**:239–260.

Table 1. Estimated parameter values for shale samples AC1, AC5, AC8

Parameter	AC1	AC5 (S1)	AC5 (S2)	AC8
n_s	10^4	10^3	10^3	3.0
β_s	1.77	1.83	1.83	2.0
$<r_{s1}>$ (nm)	17.20	22.80	22.80	5.61
σ_{s1}(nm)	28.93	10.88	10.88	5.56
$<r_{s1}>$ (nm)	1.93	3.78	3.78	1.29
σ_{s1} (nm)	0.61	1.14	1.14	0.2
c_s	0.248	0.356	0.356	0.140
$<r_s>$ (nm)	5.73	10.55	10.55	1.89
σ_s (nm)	15.9	11.22	11.22	2.57
$<r_{b1}>$ (nm)	3.21	20.2	30.53	6.65
σ_{b1} (nm)	7.58	9.63	24.19	97.37
$<r_{b2}>$ (nm)	1.87	4.15	3.79	1.12
σ_{b2} (nm)	0.64	1.61	1.43	0.2
c_b	0.295	0.503	0.568	0.1438
$<r_b>$ (nm)	2.26	12.22	18.98	1.91
σ_b (nm)	4.22	10.74	22.63	3.69
q_{bc0}	$5.8x10^{-4}$	0.1278	0.1079	0.0279
θ_{Hg}	65°	40.3°	40.3°	65°
V_p (cm^3/g)	0.0164	0.0132	0.0132	0.0174

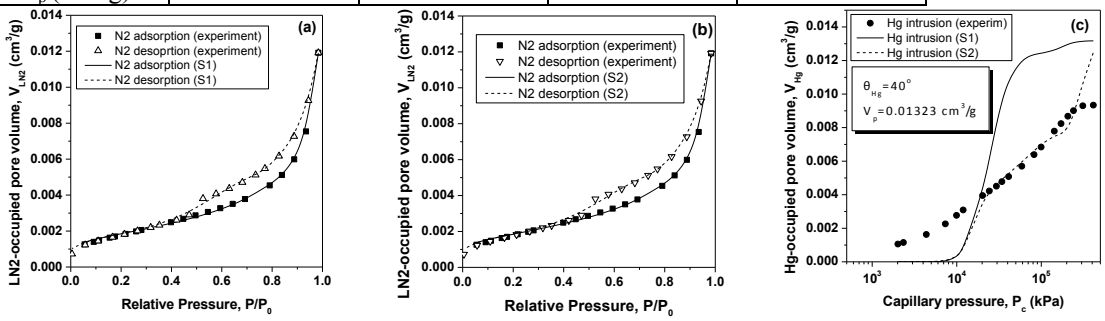

Figure 1. Measured (AC5) vs predicted (a) N2 sorption isotherms (simulated structure S1), (b) N2 sorption isotherms (simulated structure S2), (b) Hg intrusion curve (simulated structures S1 & S2)

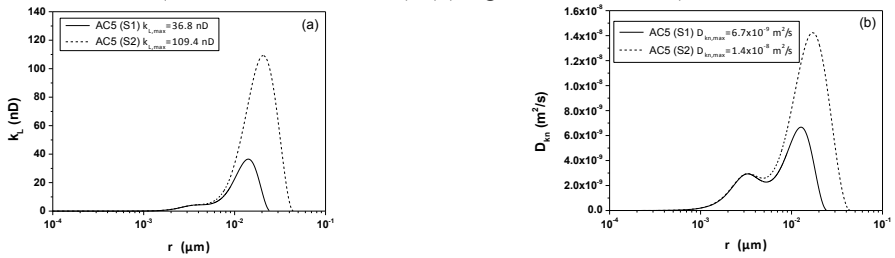

Figure 2. (a) Liquid permeability, and (b) Knudsen diffusion coefficient of the critical path as a function of throat radius for two simulated pore structures (S1,S2) of sample AC5

Table 2. Comparison of predicted vs experimentally measured flow properties of shales

Shale sample	AC1	AC5	AC5	AC8
$(k_L)_{exp}$ (nD)	$3x10^{-4}$	61.0	61.0	6.6
$(k_L)_{pred}$ (nD)	0.158	36.8 (S1)	109.4 (S2)	0.6
$(D_{kn})_{exp}=(bk_L/\mu_g)_{exp}$ (m^2/s)	$2.26x10^{-10}$	$7.7x10^{-9}$	$7.7x10^{-9}$	$1.7x10^{-9}$

$(D_{kn})_{pred}$ (m^2/s)	$2.77x10^{-10}$	$6.7x10^{-9}$ (S1)	$1.4x10^{-8}$ (S2)	$1.6x10^{-9}$
$\lambda/<r_s>$	10.5	5.7	5.7	31.6